

Geochemical and Nd isotopic constraints on the origin of uppermost Silurian rhyolitic rocks in the northern Appalachians (northern New Brunswick): tectonic implications

Tracking no: BK659-APPALACHIAR

Authors:

Jaroslav Dostal (Saint Mary's University), Pierre Jutras (Saint Mary's University), and Reginald Wilson (University of New Brunswick)

Abstract:

Voluminous bimodal volcanic rocks of the Silurian (~422 - 420 Ma) Dickie Cove Group in the Ganderia domain of northern New Brunswick, Canada, are subaerial units that were deposited in an extensional setting, with the mafic types corresponding to continental tholeiites. Felsic rocks are rhyolites with calc-alkaline affinities. They exhibit geochemical characteristics that are typical of A2-type felsic magmas, such as enrichments in the incompatible elements Zr, Nb and Y, as well as high FeO*/(FeO*+MgO) and Ga/Al ratios. Their $\epsilon\text{Nd}(t)$ values are positive (+0.7 to 3.4), but lower than those of the associated basalts. Saturation thermometry has yielded average zircon crystallization temperature estimates for the rhyolites that are well above 900°C. The geochemical data indicate that the felsic melts were likely sourced from heterogeneous, Neoproterozoic lower crust, and generated by dehydration melting triggered by heat derived from underplated mafic magma. Parent melts of the rhyolites underwent fractional crystallization in a complex magma chamber prior to eruption. The Nd isotopic data suggest that the lower crust of Ganderia is similar to that of Avalonia in northern mainland Nova Scotia, and that the two microcontinents share a common Neoproterozoic history and origin as continental blocks rifted from neighboring parts of Gondwana. The tectono-magmatic setting of the Dickie Cove Group volcanic rocks is interpreted as being related to Pridolian, post-Salinic relaxation and slab breakoff, which generated volcanism initially constrained within the Chaleur Zone of the Chaleur Bay Synclinorium, a large domain of the northern Appalachians. This was followed later in the Pridolian by extensional collapse and widening of the area of magmatic activity, which then prograded into the Tobique Zone farther to the southwest.

25

26 **Abstract**

27

28 Voluminous bimodal volcanic rocks of the Silurian (~422 - 420 Ma) Dickie Cove Group
29 in the Ganderia domain of northern New Brunswick, Canada, are subaerial units that
30 were deposited in an extensional setting, with the mafic types corresponding to
31 continental tholeiites. Felsic rocks are rhyolites with calc-alkaline affinities. They exhibit
32 geochemical characteristics that are typical of A2-type felsic magmas, such as
33 enrichments in the incompatible elements Zr, Nb and Y, as well as high $\text{FeO}^*/$
34 $(\text{FeO}^* + \text{MgO})$ and Ga/Al ratios. Their $\epsilon_{\text{Nd}}(t)$ values are positive (+0.7 to 3.4), but lower
35 than those of the associated basalts. Saturation thermometry has yielded average zircon
36 crystallization temperature estimates for the rhyolites that are well above 900°C. The
37 geochemical data indicate that the felsic melts were likely sourced from heterogeneous,
38 Neoproterozoic lower crust, and generated by dehydration melting triggered by heat
39 derived from underplated mafic magma. Parent melts of the rhyolites underwent
40 fractional crystallization in a complex magma chamber prior to eruption. The Nd isotopic
41 data suggest that the lower crust of Ganderia is similar to that of Avalonia in northern
42 mainland Nova Scotia, and that the two microcontinents share a common Neoproterozoic
43 history and origin as continental blocks rifted from neighboring parts of Gondwana. The
44 tectono-magmatic setting of the Dickie Cove Group volcanic rocks is interpreted as being
45 related to Pridolian, post-Salinic relaxation and slab breakoff, which generated volcanism
46 initially constrained within the Chaleur Zone of the Chaleur Bay Synclinorium, a large
47 domain of the northern Appalachians. This was followed later in the Pridolian by

48 extensional collapse and widening of the area of magmatic activity, which then prograded
49 into the Tobique Zone farther to the southwest.

50

51

52 **Introduction**

53

54 The Appalachian orogenic belt extends for more than 3,000 km along the eastern
55 margin of North America from Alabama in the southern United States to Newfoundland
56 in the north. The northern Appalachian Orogen underwent a protracted and complex
57 tectonic evolution that led to a collage of accreted terranes sandwiched between the
58 Laurentian and Gondwanan cratonic and peri-cratonic domains (Fig. 1). The orogen
59 formed during the early Paleozoic closure of Iapetus (proto-Atlantic Ocean) and of
60 several marginal seaways and basins. This led to the accretion of intra-oceanic and
61 continental margin arcs and microcontinents that were located in the Iapetus Ocean (e.g.,
62 Pollock et al., 2012; van Staal and Barr, 2012; Wilson et al., 2017). Later stages of
63 Iapetus closure are characterized by the accretion of two peri-Gondwanan
64 microcontinents, Ganderia and Avalonia, which docked during the middle Paleozoic prior
65 to the accretion of the Gondwanan continent (e.g., van Staal and Barr, 2012). However,
66 the nature, timing and modes of accretion of these microcontinents are still debated. For
67 example, there is even disagreement on whether or not Ganderia and Avalonia represent
68 distinct terranes (e.g., van Staal and Hatcher, 2010; Keppie et al., 2012; Waldron et al.,
69 2014).

70 Voluminous Silurian to Lower Devonian bimodal (mafic-felsic) volcanic rocks
71 form part of an overstep sequence on the accreted vestiges of Iapetus at the margin of
72 composite Laurentia. Study of these rocks can be critical for the understanding of
73 accretionary/tectonic processes along the northern Appalachian Orogen and can also
74 provide insights regarding the evolution of continental crust. This paper presents whole-
75 rock major and trace element data as well as isotopic data from bimodal volcanic rocks of
76 the Silurian Dickie Cove Group (formerly part of the Chaleur Group) in northern New
77 Brunswick, with a focus on the felsic rocks, in order to (1) discuss their petrogenesis and
78 (2) constrain their tectonic and geodynamic settings in the context of Iapetus Ocean
79 closure.

80

81

82 **Geological Setting**

83

84 A prominent feature of the northern Appalachians, the Matapedia cover sequence
85 (MCS) is a large Middle Paleozoic successor (overstep) basin-fill that was deposited
86 across the accreted vestiges of Iapetus on composite Laurentia (Fig. 2). The MCS
87 unconformably overlies Ordovician rocks of the Ganderian Popelogan arc and
88 Tetagouche-Exploits back-arc basin (van Staal et al., 2009). It extends from the Gaspé
89 Peninsula of eastern Quebec to central Maine, and underlies a large part of northern New
90 Brunswick.

91 The MCS consists of three structural zones (Fig. 2), which are, from northwest to
92 southeast, the Connecticut Valley-Gaspé Synclinorium, the Aroostook-Percé

93 Anticlinorium, and the Chaleur Bay Synclinorium (Rodgers, 1970; Wilson et al., 2004).
94 The Chaleur Bay Synclinorium records extensive magmatic activity that immediately
95 post-dates Silurian closure of the Tetagouche-Exploits back-arc basin and breakoff of the
96 Tetagouche-Exploits lithosphere during the Salinic orogenic cycle. Closure of the back-
97 arc basin is also responsible for the Upper Ordovician to Silurian formation of the
98 Brunswick subduction complex, an accretionary wedge (van Staal et al., 2009; Wilson et
99 al., 2017). The Chaleur Bay Synclinorium is divided into two parts by the WSW-ENE
100 trending Rocky Brook-Millstream Fault (Fig. 2). The northern part (the Chaleur Zone)
101 contains two prominent subaerial to subaqueous post-Salinic volcanic suites hosted by
102 the Pridolian (Silurian) Dickie Cove Group and the Lochkovian to lowermost Emsian
103 (Lower Devonian) Dalhousie Group (Fig. 2C).

104 The dominantly volcanic rocks of the Dickie Cove Group (DCG) (*sensu* Wilson
105 and Kamo, 2012) were formerly assigned to the Chaleur Group by Irrinki (1990) and
106 Walker and McCutcheon (1995). The DCG is composed of bimodal (mafic-felsic)
107 volcanic rocks and minor associated volcanogenic sedimentary rocks. The upper part of
108 the group (Benjamin Formation) predominantly consists of aphyric to feldspar-phyric
109 rhyolites and felsic pyroclastic rocks (lithic tuff, lithic-crystal tuff and ignimbrite). Mafic
110 volcanic and coarse-grained pyroclastic rocks are subordinate lithotypes. Facies of the
111 felsic rocks are typical of volcanic rocks emplaced in subaerial environments. The DCG
112 was dated by Wilson and Kamo (2008, 2012), who obtained a U-Pb zircon age of
113 422.3 ± 0.3 Ma from the base of the group, and 419.7 ± 0.3 Ma from the top. The DCG
114 unconformably overlies Silurian sedimentary rocks (Quinn Point Group) and is
115 disconformably overlain by the Lower Devonian Dalhousie Group (Fig. 2C), which

116 comprises interbedded shallow marine sedimentary rocks as well as subaerial to shallow
117 marine mafic and subordinate felsic effusive and pyroclastic rocks.

118 The southern part of the Chaleur Bay Synclinorium (the Tobique Zone) includes
119 the Pridolian to Lochkovian Tobique Group (TG), which contains sedimentary rocks as
120 well as abundant mafic and felsic volcanic rocks (Wilson et al., 2017; Dostal et al. 1989,
121 2016, 2020). Biostratigraphic and U-Pb zircon ages show that deposition of the TG
122 overlaps that of both the Dickie Cove and Dalhousie groups (Wilson and Kamo, 2008),
123 with the volcanic-dominated lower part of the Tobique Group correlating with the DCG,
124 and the sedimentary-dominated upper part correlating with the Dalhousie Group. In the
125 northern part of the Tobique Zone, near its faulted boundary with the Chaleur Zone, a
126 continuous succession of Ludlovian to Lockhovian sedimentary rocks (Petit Rocher
127 Group and Greys Gulch Formation; Fig. 2C) is conformably overlain by marine
128 sedimentary rocks and subordinate subaqueous volcanic rocks of the upper part of the TG
129 (Wilson, 2017), implying that the dominantly volcanic Pridolian successions of the DCG
130 and basal TG belong to two distinct and geographically separated suites.

131

132

133 **Petrography**

134

135 Rhyolitic volcanic rocks of the DCG are massive to flow-banded, aphyric to
136 porphyritic, and locally vesicular. The matrix of the volcanic rocks is fine-grained or
137 glassy, and vitrification textures are common. Feldspar phenocrysts are euhedral to
138 subhedral, whereas rare quartz phenocrysts are embayed. Biotite and Fe-Ti oxides are

139 rare, and zircon, apatite and monazite are accessory minerals. The volcanic rocks
140 underwent low-grade metamorphism of zeolite to lower greenschist facies, as indicated
141 by mineral assemblages in the associated mafic rocks (Dostal et al., 1989; Mossman and
142 Bachinski, 1972). Their primary mineral assemblages are variable, but extensively
143 replaced by secondary minerals such as sericite and chlorite. Typically, their K-feldspar
144 fraction is sericitized, and their plagioclase fraction is saussuritized.

145

146

147 **Analytical Methods**

148

149 The analyzed felsic volcanic rocks were selected from a collection of more than
150 one hundred samples collected during regional mapping of the DCG (e.g., Wilson et al.
151 2005; Wilson, 2017). Whole-rock major and trace elements were analyzed at the
152 Activation Laboratories Ltd. in Ancaster, Ontario, Canada. An inductively-coupled
153 plasma-optical emission spectrometer was used for the analysis of major elements,
154 whereas trace element contents were determined by inductively-coupled plasma mass
155 spectrometry. Based on analytical results obtained from international standard rocks, the
156 analytical precision and accuracy were typically better than 5% for major elements and
157 better than 10% for trace elements.

158 Sm and Nd contents as well as Nd isotope ratios were determined at the Atlantic
159 Universities Regional Isotope Facility of the Department of Earth Sciences at Memorial
160 University of Newfoundland (St. John's, Newfoundland, Canada) by a multicollector
161 Finnigan MAT 262 thermal ionization mass spectrometer (Pollock et al., 2015). During

162 the course of data acquisition, replicates of the JNdi-1 standard gave a mean value of
163 $^{143}\text{Nd}/^{144}\text{Nd} = 0.512100 \pm 0.000007$ (2σ , $n=21$). All reported values for the samples were
164 adjusted to the value of the JNdi-1 standard ($^{143}\text{Nd}/^{144}\text{Nd}_{\text{certified}} = 0.512115 \pm 7$). The 2σ
165 values for $^{143}\text{Nd}/^{144}\text{Nd}$ ratios are given in Table 1. Initial Nd isotope ratios and epsilon
166 values (ϵ_{Nd}) were corrected using the age of 421 Ma (Table 1). T_{DM} model ages (Table 1)
167 were calculated in accordance with DePaolo (1988).

168

169

170 **Geochemistry**

171

172 *Alteration*

173

174 As noted earlier, rocks of the DCG were modified by secondary processes that
175 might have changed the concentration of mobile elements, including K_2O and Na_2O .
176 Some samples were also hydrothermally altered. Several strongly altered samples were
177 eliminated. The remaining samples show consistent variations of immobile- and mobile-
178 element patterns on various diagrams, suggesting that most element variations are likely
179 related to magmatic processes. Furthermore, to limit the problem of alteration, the
180 interpretations in this paper are based mainly on elements that are generally considered to
181 be little affected by secondary processes, such as rare-earth elements (REE) and high-
182 field-strength elements (HFSE).

183

184

185 *Major and Trace Elements*

186

187 Volcanic rocks of the DCG range from basalts to rhyolites, with rare intermediate
188 rock-types, implying that the suite is bimodal. Wilson (2017) estimated that rocks with <
189 52% silica constitute >30% of the suite, whereas rocks with >68% silica represent ~ 52%
190 of the suite. The DCG mafic rocks are continental tholeiitic basalts and subordinate
191 basaltic andesites (Dostal et al., 2016), but the felsic rocks are only poorly known. The
192 DCG rhyolites have silica ranging from ~ 68% to 77% and plot mainly within the
193 rhyolite field on the Zr/TiO₂ versus Nb/Y classification diagram (Fig. 3). The felsic rocks
194 have high Fe* (FeO*/FeO*+MgO) values (Fig. 4) and are ferroan (Frost et al., 2001).
195 Overall, the rocks have low contents of CaO, TiO₂, MgO and FeO*, but high contents of
196 alkalis, which are characteristics of A-type felsic rocks. The rocks also show weak
197 negative correlations of Al₂O₃, TiO₂, MgO, FeO* and CaO with increasing silica, which
198 is broadly consistent with the fractionation of ferromagnesian minerals, Fe-Ti oxides and
199 calcic plagioclase. Consistent with the rift-related signature of associated basalts in the
200 group (Dostal et al., 2016), the DCG felsic rocks plot into the A-type granite fields (Fig.
201 5).

202 The chondrite-normalized REE patterns of the felsic rocks display slight
203 enrichment in light REE (LREE), but flat heavy REE (HREE) accompanied by negative
204 Eu anomalies (Fig. 6). The (La/Yb)_n ratios vary between 3.5 and 8.5, whereas (Tb/Yb)_n
205 ratios are between 1 and 1.5. The patterns are generally parallel to subparallel. The
206 variably pronounced negative Eu anomalies reflect feldspar fractionation and suggest low
207 oxygen fugacity in the felsic melt. The relatively flat HREE patterns imply the absence of

208 garnet at the source of these rhyolites, indicating an origin at relatively low pressures and
209 at a depth that is shallower than the garnet stability field, which starts at a depth of ~60-
210 80 km (McKenzie and O’Nions, 1991). Unlike those of the rhyolites, REE patterns in the
211 associated basalts of the group are linear, negative Eu anomalies are absent, and HREE
212 define a steeper slope $[(Tb/Yb)_n \sim 2]$ (Fig. 6B; Dostal et al., 2016).

213 According to their primitive mantle-normalized patterns, the felsic rocks are more
214 enriched in both highly and moderately incompatible elements than the basalts (Fig. 7).
215 The rhyolites display depletion in Ba, Sr, Ti and Eu, which suggests fractionation of
216 feldspars and Fe-Ti oxides (Fig. 7), and which contrasts with the basalts. The felsic rocks
217 also show negative Nb and Ta anomalies. The trace element patterns of some of these
218 rocks resemble those of the continental crust (e.g., Rudnick and Gao, 2003).

219

220

221 *Isotopes*

222

223 $\epsilon_{Nd}(t)$ values for the DCG rhyolites range from +0.73 to +3.37 ($t=421$ Ma). These
224 values are notably higher than those of felsic volcanic rocks in the Tobique Zone (Dostal
225 et al. 2020), but they are on average lower than those of the associated basalts (Table 1).
226 They are also lower than values for the contemporaneous depleted mantle. The depleted
227 mantle model age (T_{DM} ; after De Paolo, 1988) of the DCG rhyolites vary between 0.7 and
228 1.0 Ga, and are slightly older than those of the basalts (0.65 - 0.8 Ga), but younger than
229 those of felsic volcanic rocks in the Tobique Group (0.9 - 1.2 Ga). The DCG rhyolites

230 also have lower $^{147}\text{Sm}/^{144}\text{Nd}$ ratios (0.1196 - 0.1337) compared to the basalts (0.1400 -
231 0.1475).

232

233

234 **Discussion**

235

236 *Zircon saturation thermometry*

237

238 The temperature of zircon saturation ($T_{\text{Zr}}^{\circ\text{C}}$) in felsic magmas has been used to
239 characterize various felsic rocks in terms of their origin and thermal history (Miller et al.,
240 2003; Dostal et al. 2015; Xia et al., 2016; Murphy et al., 2018). For example, Miller et al.
241 (2003) differentiate “hot” granites, which are assumed to be generated by anhydrous
242 melting at high temperature ($T_{\text{Zr}} > 800^{\circ\text{C}}$), from “cold” granites ($T_{\text{Zr}} < 800^{\circ\text{C}}$), which were
243 derived from a crustal source in water-fluxed settings (Collins et al., 2016). The
244 temperature at which zircon starts to crystallize is related to major element composition
245 as well as Zr concentrations. The relationship was tested experimentally and is expressed
246 by the M value of Watson and Harrison (1983). Within an experimental range of M
247 values (i.e. $M=1.3 - 1.9$), the temperature estimates may be useful for petrogenetic
248 considerations (Hanchar and Watson, 2003; Collins et al., 2016). Values of M, as
249 calculated in accordance with Boehnke et al. (2013), are within the experimental range of
250 Watson and Harrison (1983) for most of the DCG felsic rocks, indicating that the rocks
251 can provide meaningful temperature estimates (Table 2). The temperature estimates range
252 from $845^{\circ\text{C}}$ to $1047^{\circ\text{C}}$, with an average value of $929^{\circ\text{C}}$ ($\pm 64^{\circ\text{C}}$ s.d.). This relatively

253 wide temperature range could in part be related to magma evolution in shallow crust
254 (fractionation, alteration, host rock assimilation). Hence, the average or maximum values
255 are considered to be more diagnostic (Murphy et al., 2018).

256 Our results suggest that the initial magmatic temperature was well above 800°C,
257 and that the DCG rhyolites therefore issued from a “hot” felsic melt (*sensu* Miller et al.,
258 2003). T_{Zr} (°C) values were also calculated for felsic volcanic rocks of the TG in order to
259 assess possible petrogenetic similarities or dissimilarities between the two suites.

260 Rhyolite samples from the TG (Dostal et al., 2020) provide temperature estimates that
261 range from 797°C to 864°C, with an average of 824°C. Results from both suites are
262 consistent with the relatively hot melting temperature of the anhydrous lower crust
263 (Huppert and Sparks, 1988; Annen et al., 2006, 2015). Although there is an overlap in
264 zircon saturation temperatures between the TG and DCG rhyolites, the latter have a
265 higher average value, which is consistent with the conclusion that the TG basalts were
266 generated at a shallower depth than those of the DCG (Dostal et al., 2016). The DCG
267 rhyolites also bear higher $\epsilon_{Nd}(t)$ values than those of the TG suites (Dostal et al., 2020),
268 which suggests that the DCG rhyolites had a larger proportion of mantle-derived material
269 at their source.

270

271 *Monazite saturation thermometry*

272

273 To verify the relatively high crystallization temperature that is estimated for the
274 DCG rhyolites, monazite saturation temperatures were calculated by relating the
275 concentration of light REE to the bulk composition of the magma. The calculations

276 (based on Montel, 1993) yielded an average temperature of 853°C (\pm 40°C) for the DCG
277 rhyolites (Table 2), which is consistent with monazite crystallization occurring after that
278 of zircon, but which still suggests a relatively high crystallization temperature. All these
279 temperature estimates are similar to modeled temperatures of partial melting of the crust
280 associated with basalt injection (Annen and Sparks, 2002).

281

282 *Petrogenesis*

283

284 Unlike Silurian (Llandoverly to Ludlow) volcanic rocks of the Coastal volcanic
285 belt in Maine and southern New Brunswick, which are typical continental arc calc-
286 alkaline suites ranging from mafic to felsic types (Llamas and Hepburn, 2013), rocks of
287 the Chaleur Bay Synclinorium farther inland are bimodal and include rift-related
288 continental tholeiites inferred to be derived from the subcontinental lithospheric mantle
289 (Dostal et al., 2016). However, the origin of the DCG rhyolitic rocks and of many other
290 felsic rocks that are part of compositionally bimodal suites has been debated.

291 Various models for the origin of bimodal suites have been discussed for decades
292 (e.g., Bowen, 1928; Barbarin, 1999; Riley et al., 2001). The two main models are based
293 on either crystal fractionation or crustal melting. The first model (e.g., Lacasse et al.
294 2007; Waight et al., 2007) assumes a derivation of felsic magma by the extensive crystal
295 fractionation of basaltic magma (up to 90%), or by a combined process of assimilation
296 and fractional crystallization. The second model invokes partial melting of crustal rocks
297 triggered by heating from underplated mantle-derived basaltic magmas (e.g., Huppert and
298 Sparks, 1988). The latter model is frequently used (e.g., Annen and Sparks, 2002) to

299 explain the formation of large felsic magma reservoirs, as fractional crystallization would
300 require an unreasonably large volume of basaltic parental magma.

301 Variations in FeO^*/MgO versus TiO_2 (Fig. 8) show that there is no obvious
302 relationship between the DCG mafic rocks, which display a typical tholeiitic fractionation
303 trend, and the DCG felsic rocks, which show a calc-alkaline trend. This and other
304 geochemical characteristics of these rocks, such as contrasting Tb/Yb and Th/Nb ratios as
305 well as significant differences in Nd isotopic values (Table 1), suggest that the felsic
306 rocks were not derived from the mafic rocks by crystal fractionation. Thus, the paucity of
307 intermediate rock types (Daly gap), large volume of felsic rocks relative to associated
308 mafic rocks, and contrasting geochemical and Nd isotopic characteristics between the two
309 rock-types are consistent with a derivation from different sources. This process can also
310 account for some compositional variations within felsic magma bodies (Altherr et al.,
311 2000; Shellnutt et al. 2011), as felsic magma heterogeneity may, in part, reflect
312 heterogeneity of the crustal source.

313 As noted earlier, the DCG felsic rocks are similar in composition to A-type (i.e.
314 within plate) granitic rocks. Eby (1992) noted that A-type granitic rocks can be
315 subdivided into at least two types. The parental magma of granites in the A1 subgroup is
316 mafic and derived from a mantle source. A1 granites have incompatible trace elemental
317 ratios that are similar to those of ocean-island basalts. The compositionally diverse A2
318 subgroup is sourced from the lithosphere, and is characterized by elemental ratios that are
319 similar to those of continental crust or island arc basalts. The DCG rhyolites have
320 affinities with A2-type granites (Fig. 9). Many such granites are considered to represent
321 magmas derived from the lower to middle crust (Eby 1992; King et al., 1997).

322 Some geochemical variation trends in the DCG rhyolitic rocks are likely related to
323 differentiation processes, particularly fractional crystallization that occurred after the
324 magma was formed. In addition to fractionation of major phases, mainly feldspars and
325 minor ferromagnesian minerals and Fe-Ti oxides, accessory minerals also played a role
326 during fractional crystallization as they control much of the REE variation. A graph of
327 $(La/Yb)_n$ versus La (Fig. 10A) suggests that fractionation of REE, the bulk of which is
328 hosted by accessory phases, was dominated by the crystallization of monazite. Although
329 fractional crystallization involved the crystallization of feldspars, variations in Ba and Sr,
330 which are elements that are preferentially hosted by feldspars, do not correlate with
331 negative Eu anomalies (Eu/Eu^*). This may indicate buffering from the activity of fluids.
332 Two distinct trends on the Ba versus Eu/Eu^* diagram (Fig. 11A) suggest the existence of
333 a complex magma chamber, although all the DCG rhyolites have similar evolutions.

334 In addition to fractional crystallization, a variable degree of partial melting can
335 also generate variations in rock composition. Schiano et al. (2010) suggested that partial
336 melting and fractional crystallization processes can be identified from systematic changes
337 in incompatible trace element concentrations and their ratios. The Ba/Zr versus Ba plot
338 (Fig. 11B) shows that some samples were derived from different degrees of partial
339 melting than the majority of the rhyolites. However, some significant compositional
340 variations in the rhyolitic rocks cannot be attributed to fractional crystallization or to a
341 variable degree of partial melting (e.g., variations in trace element ratios and Nd isotopic
342 values), but rather point to a heterogeneous source. The Th/Nb versus Zr graph (Fig.
343 10B) is useful for an evaluation of source heterogeneity: Th/Nb, which is not
344 significantly affected by fractional crystallization, is plotted against an incompatible trace

345 element (Zr) that increases in concentration with fractionation. The variation in Th/Nb
346 ratios (Fig. 10B) therefore likely reflect crustal source heterogeneity for the DCG
347 rhyolites. The plot also implies that assimilation-fractional crystallization (AFC)
348 processes, which lead to an enrichment trend that is intermediate between fractional
349 crystallization and source heterogeneity vectors, do not appear to have played a
350 significant role in the genesis of the rhyolites.

351 The DCG rhyolitic rocks likely represent melts that were derived from crustal
352 material. This conclusion is also supported by their distribution patterns in primitive
353 mantle normalized plots, which display depletions in Nb, Ta, Ti, Eu, Ba, and Sr (Fig. 7),
354 altogether indicating that the DCG felsic rocks have been sourced from continental crust.
355 Nd model ages for the DCG rhyolites are Neoproterozoic (Table 1), which is consistent
356 with the age of Ganderian basement rocks (van Staal et al., 1996, 2012; Dostal et al.,
357 2016, 2020; Fig. 12). Moreover, the $\epsilon_{Nd}(t)$ values overlap the isotope envelope of
358 Avalonian crustal values (Fig. 12), which suggests that Ganderia and Avalonia have a
359 common Neoproterozoic history and a similar lower/middle crust (Dostal et al., 2020).
360 The Nd isotopic data also shows that the crustal source of the DCG rhyolites was similar
361 but distinct from that of the TG rhyolites.

362 Murphy et al. (2018) argued that partial melting of an anhydrous lower crustal
363 source produced the A-type magmas of northern Nova Scotia, in West Avalonia. A
364 similar process and source can be invoked for the DCG rhyolites. Partial melting of
365 various crustal reservoirs has been invoked to explain the chemical characteristics of “A-
366 type” felsic rocks, such as a charnockitic lower crust, an I-type granite precursor, calc-
367 alkaline amphibole-bearing tonalite, mafic underplated rocks, and some others (e.g.,

368 Collins et al., 1982; Creaser et al., 1991; King et al., 1997; Bonin, 2007). Dostal et al.
369 (2020) inferred that partial melts of granodioritic/tonalitic and charnockitic rocks or their
370 sedimentary or metamorphic equivalents have a major element composition that is
371 similar to that of the A2-type TG felsic volcanic rocks, and that either could represent the
372 parent material. Similar crustal source possibilities can be suggested for the DCG felsic
373 rocks. The continental crust is compositionally diverse and includes both juvenile and
374 recycled material. The Neoproterozoic T_{DM} values for the DCG rhyolites suggest an
375 ancient source that probably experienced episodic recycling, such as in a subduction zone
376 or at the root of a continent-continent collision. Eby (1992) suggested that these processes
377 may contribute to the “within-plate” signature of A2-type felsic rocks.

378 Continental crust can melt as a result of repeated injections of hot mafic magmas
379 (Huppert and Sparks, 1988; Annen and Sparks, 2002; Annen et al. 2006). The
380 temperature of the crust may exceed 800°C during continuous basalt injection - hot
381 enough to create partial melts (Annen and Sparks, 2002). Thus, rising mafic magma may
382 have triggered melting of the crust from which the felsic rocks inherited their
383 geochemical characteristics. This process is common during lithospheric extension and is
384 a consequence of magmatic underplating (e.g. Huppert and Sparks, 1988). Hence, dry
385 partial melting of the heterogeneous lower crust of Ganderia most likely produced the
386 primary melt that sourced the DCG rhyolites. However, prior to its eruption, this primary
387 melt may have resided in plutonic bodies such as the compositionally similar and almost
388 coeval Landry Brook and Dickie Brook plutons, which intrude the DCG in the Chaleur
389 Zone (Fig. 2) (Pilote et al., 2013; Wilson and Kamo, 2016).

390

391

392 **Tectonic Setting**

393

394 Following accretion of Ganderia's leading edge (the Popelogan arc) to Laurentia
395 in the Upper Ordovician, the Tetagouche-Exploits back-arc basin that separated
396 Ganderia's leading and trailing segments began to close, culminating with the ~425 Ma
397 Salinic Orogeny (van Staal et al., 2009; Zagorevski et al., 2010; Wilson et al., 2017) (Fig.
398 13 A, B). At 422.3 ± 0.3 Ma (Wilson and Kamo, 2008), the DCG provides some of the
399 earliest record of extrusions related to post-Salinic extensional magmatism (*sensu* Dostal
400 et al., 2020) in the northern Appalachians. A possible equivalent is the Stony Lake
401 Rhyolite, which lies above the Salinic unconformity in Newfoundland, and which was
402 roughly dated at 423^{+3}_{-2} Ma by Dunning et al. (1990). This volcanism has been
403 associated with post-orogenic relaxation and breakoff of the Tetagouche-Exploits slab
404 (van Staal et al., 2009; Wilson et al., 2017) (Fig. 13C). Mafic eruptions in the DCG may
405 be linked to the ponding of asthenospheric melt in the rising root of the orogen, which
406 resulted in high-degree partial melting of the subcontinental lithospheric mantle (Dostal
407 et al., 2016) (Fig. 13C). Evidence for high heat flow during generation of the DCG felsic
408 melts suggests that its lower crustal source was located in the focus zone of mafic
409 upwelling and crustal underplating (Fig. 13C). Because it was associated with a post-
410 orogenic rise of the lithosphere, initial post-Salinic magmatism was subaerial and limited
411 in extent to a narrow, orogen-parallel belt.

412 In New Brunswick, volcanism in the early part of the Pridolian was constrained to
413 the Chaleur Zone (Wilson et al., 2017). Later in the Pridolian, extensional collapse of the

414 orogenic root (van Staal and de Roo, 1995) resulted in a widening of both the sub-
415 lithospheric and sub-crustal areas of underplating. This led to an expansion of the area of
416 volcanism into the Tobique Zone, thus triggering the onset of TG volcanism (418.6 -
417 420.8 Ma; Wilson et al, 2017) in a separate volcanic centre (Fig. 13D). Although these
418 two zones are currently located roughly along-strike from each other, it is inferred that
419 the Chaleur Zone lay farther west in relation to the Tobique Zone prior to post-Silurian
420 dextral faulting along the Rocky Brook-Millstream fault system (Wilson, 2017).
421 However, emplacement of both volcanic belts was originally parallel to the southwest-
422 northeast-trending Salinic grain of the orogen (Fig. 13D).

423 Evidence for lower heat flow during generation of the TG felsic melts compared
424 to the DCG melts suggests that the lower crustal source of the TG volcanic rocks was
425 located farther away from the locus of mafic upwelling and crustal underplating (Fig.
426 13D). This is consistent with Nd isotopic data, which imply that felsic rocks of the DCG
427 and TG issued from two slightly distinct crustal sources.

428

429

430 **Conclusions**

431

432 Following the Wenlock-Ludlow Salinic Orogeny (Fig. 13A, B), post-orogenic
433 relaxation and breakoff of the Tetagouche-Exploits slab resulted in the development of
434 extensional tectonics in Ganderian rocks of the northern Appalachian orogen, and
435 eventually led to the emplacement of Pridolian to lowermost Emsian bimodal suites in a
436 discontinuous, orogen-parallel belt stretching from Maine to eastern Quebec. The ~422 -

437 420 Ma Dickie Cove Group of northern New Brunswick provides the earliest record of
438 this long period of extensional volcanism, which, in the early part of the Pridolian, was
439 constrained to the Chaleur Zone in the northern part of the Chaleur Bay Synclinorium
440 (Fig. 13C).

441 Rhyolites are the dominant felsic rock type in the voluminous bimodal volcanic
442 suite of the Dickie Cove Group. Geochemical evidence suggests that these felsic rocks,
443 which show a calc-alkaline trend, were not produced by fractional crystallization of
444 associated mafic melts, which show a tholeiitic trend. The geochemical data indicate that
445 the felsic melts, which plot as “within-plate”, A2-type melts on various discrimination
446 diagrams, were likely sourced from heterogeneous, Neoproterozoic lower crust, and that
447 they were generated by dehydration melting triggered by heat derived from the associated
448 mafic magma. Saturation thermometry has yielded average zircon and monazite
449 crystallization temperature estimates for the rhyolitic rocks that are well above 900°C and
450 800°C, respectively. Parent melts of the DCG rhyolites underwent fractional
451 crystallization in a complex of magma chambers prior to erupting in sub-aerial
452 conditions.

453 The $\epsilon_{\text{Nd}}(t)$ values of the DCG rhyolites are positive (+0.73 to +3.37), but lower
454 than those of the associated basalts. Nd model ages are Neoproterozoic (0.7 - 1.0 Ga),
455 which is typical of Ganderian and Avalonian crust. The data also suggest that the lower
456 crust of Ganderia is similar to that of Avalonia in northern mainland Nova Scotia. This is
457 consistent with Nd isotopic data from some Silurian to Lower Devonian granitic and
458 felsic rocks in other areas of Ganderia (e.g., Whalen et al., 1994, 1996), which also plot
459 into the Avalonian envelope (Fig. 12; Dostal et al., 2020). The similarity of lower crust

460 composition in both microcontinents suggests a common Neoproterozoic history and is
461 consistent with their inferred origin as continental blocks rifted from neighboring parts of
462 Gondwana (e.g., van Staal and Barr, 2012; van Staal et al., 2012; Waldron et al., 2014).

463

464

465 **Acknowledgements**

466

467 This research was supported by NSERC (Canada) Discovery grants to J.D and P.J. and
468 by New Brunswick Department of Energy and Resource Development, Geological
469 Surveys Branch. We thank reviewers Jeff Pollock and Joe Whalen, as well as co-editor
470 Brendan Murphy for constructive reviews that significantly improved this manuscript.

471

472

473 **References**

474

475 Altherr, R., Holl, A., Hegner, E., Langer, C., Kreuzer, H., 2000. High-potassium, calc-
476 alkaline I-type plutonism in the European Variscides: northern Vosges (France) and
477 northern Schwarzwald (Germany). *Lithos* 50, 487-533.

478

479 Annen C., Sparks, R.S.J., 2002. Effects of repetitive emplacement of basaltic intrusions
480 on thermal evolution and melt generation in the crust. *Earth Planetary Science Letters*
481 203, 937-955.

482

- 483 Annen, C., Blundy, J.D., Sparks, R.S.J., 2006. The genesis of intermediate and silicic
484 magmas in deep crustal hot zones. *Journal of Petrology* 47, 505-539.
485
- 486 Annen, C., Blundy, J.D., Leuthold, J., Sparks, R.S.J., 2015. Construction and evolution of
487 igneous bodies: towards an integrated perspective of crustal magmatism. *Lithos* 230, 206-
488 221.
489
- 490 Barbarian, B., 1999. A review of the relationships between granitoid types, their origins
491 and their geodynamic environments. *Lithos* 46, 605-626.
492
- 493 Boehnke, P., Watson, E.B., Trail, D., Harrison, T.M., Schmitt, A.K., 2013. Zircon
494 saturation revisited. *Chemical Geology* 351, 324-334.
495
- 496 Bonin, B., 2007. A-type granites and related rocks: evolution of a concept, problems and
497 prospects. *Lithos* 97, 1-29.
- 498 Bowen, N.L., 1928. *Evolution of Igneous Rocks*. Princeton University Press, Princeton.
499
- 500 Collins, W.J., Huang, H.Q., Jiang, X., 2016. Water-fluxed crustal melting produces
501 Cordilleran batholiths. *Geology* 44, 143-146.
502
- 503 Collins, W.J., Beams, S.D., White, A.J.R., Chappell, B.W., 1982. Nature and origin of A-
504 type granites with particular reference to southeastern Australia. *Contributions to*
505 *Mineralogy and Petrology* 80, 189-200.

506

507 Creaser, R. A., Price, R.C., Warmald, R. J., 1991. A-type granites revisited: Assessment
508 of a residual-source model. *Geology* 19, 163-166.

509

510 DePaolo, D.J., 1988. *Neodymium Isotope Geochemistry: An Introduction*: Berlin,
511 Springer Verlag, 187 p.

512

513 Dostal, J., Wilson, R.A., Keppie, J.D., 1989. Geochemistry of Siluro-Devonian Tobique
514 volcanic belt in northern and central New Brunswick (Canada): tectonic implications.
515 *Canadian Journal of Earth Sciences* 26, 1282-1296.

516

517 Dostal, J., Owen, J.V., Shellnutt, J.G., Keppie, J.D., Gerel, O., Corney, R., 2015.
518 Petrogenesis of the Triassic Bayn-Ulan alkaline granitic pluton in the North Gobi rift of
519 central Mongolia: implications for the evolution of the Early Mesozoic granitoid
520 magmatism in the Central Asian Orogenic Belt. *Journal of Asian Earth Sciences* 109, 50-
521 62.

522

523 Dostal, J., Keppie, J.D., Wilson, R.A., 2016. Nd isotopic and trace element constraints on
524 the source of Silurian-Devonian mafic lavas in the Chaleur Bay Synclinorium of New
525 Brunswick (Canada): Tectonic implications. *Tectonophysics* 681, 364-375.

526

527 Dostal, J., Wilson, R.A., Jutras, P., 2020. Petrogenesis of Siluro-Devonian rhyolites of
528 the Tobique Group in the northwestern Appalachians (northern New Brunswick,

529 Canada): Tectonic implications for the accretion history of peri-Gondwanan terranes
530 along the Laurentian margin. Geological Society of London, Special Publication (in
531 press).
532

533 Dunning, G.R., O'Brien, S.J., Colman-Sadd, S.P., Blackwood, R.F., Dickson, W.L.,
534 O'Neill, P.P., Krogh, T.E., 1990. Silurian Orogeny in the Newfoundland Appalachians.
535 *Journal of Geology* 98, 895-913.
536

537 Eby, N., 1992. Chemical subdivision of the A-type granitoids: petrogenetic and tectonic
538 implications. *Geology* 20, 641-644.
539

540 El-Bialy, M.Z., Hassen, I.S., 2012. The late Edicaran (580-590 Ma) onset of anorogenic
541 alkaline magmatism in the Arabian-Nubian Shield: Katherina A-type rhyolites of Gabal
542 Ma'ain, Sinai, Egypt. *Precambrian Research* 216-219, 1-22.
543

544 Frost, B.R., Barnes, C.G., Collins, W.J., Arculus, R.J., Ellis, D.J., Frost, C.D., 2001. A
545 geochemical classification for granitic rocks. *Journal of Petrology* 42, 2033-2048.
546

547 Hanchar, J.M., Watson, E.B., 2003. Zircon saturation thermometry. *Reviews in*
548 *Mineralogy and Geochemistry* 53, 89-112.
549

550 Huppert, H.E., Sparks, R.S.J., 1988. The generation of granite magmas by intrusions of
551 basalts into continental crust. *Journal of Petrology* 29, 599-624.

552

553 Irrinki, R.R., 1990. Geology of the Charlo area; Restigouche Count, New Brunswick.
554 Report of Investigations, New Brunswick, Mineral Resources Branch, Report 24, 118 p.

555

556 Keppie, J. D., Dostal, J., Murphy, J. B., Cousens, B. L., 1997. Palaeozoic within-plate
557 volcanic rocks in Nova Scotia (Canada) reinterpretation: isotopic constraints on
558 magmatic source and paleocontinental reconstructions. *Geological Magazine* 134, 425-
559 447.

560

561 Keppie, J.D., Murphy, J.B., Nance, R.D., Dostal, J., 2012. Mesoproterozoic Oaxaquia-
562 type basement in peri-Gondwanan terranes of Mexico, the Appalachians and Europe:
563 TDM age constraints on extent and significance. *International Geology Review* 54, 313-
564 324.

565

566 King, P.L., White, A.J.R., Chappell, B.W., Allen, C.M., 1997. Characterization and
567 origin of aluminous A-type granites from the Lachlan fold belt, southeastern Australia.
568 *Journal of Petrology* 38, 371-391.

569

570 Lacasse, C., Sigurdsson, H., Carey, S.N., Johannesson, H., Thomas, I.E., Rogers, N.W.,
571 2007. Bimodal volcanism at the Krafla subglacial caldera, Iceland: insight into the
572 geochemistry and petrogenesis of rhyolitic magmas. *Bulletin of Volcanology* 69, 373-
573 399.

574

- 575 Llamas, A.P., Hepburn J.C., 2013. Geochemistry of Silurian-Devonian volcanic rocks in
576 the Coastal Volcanic belt, Machias-Eastport area, Maine: Evidence for a pre-Acadian arc.
577 Geological Society of America Bulletin 125, 1930-1942.
578
- 579 McKenzie, D.P., O’Nions, R.K., 1991. Partial melt distributions from inversion of rare
580 earth element concentrations. *Journal of Petrology* 32, 1021-1091.
581
- 582 Miller, C.F., McDowell, S.M., Mapes, R.W., 2003. Hot and cold granites? Implications
583 of zircon saturation temperatures and preservation of inheritance. *Geology* 31, 529-532.
584
- 585 Miyashiro, A., 1974. Volcanic rock series in island arcs and active continental margins.
586 *American Journal of Science* 274, 321-355.
587
- 588 Montel, J.M., 1993. A model for monazite/melt equilibrium and application to the
589 generation of granitic magmas. *Chemical Geology* 110, 127-146.
590
- 591 Mossman, D.J., Bachinski, D. J., 1972. Zeolite facies metamorphism in the Silurian-
592 Devonian fold belt of northeastern New Brunswick. *Canadian Journal of Earth Sciences*
593 9, 1703-1709.
594
- 595 Murphy, J.B., Dostal, J., Keppie, J.D., 2008. Neoproterozoic-Early Devonian magmatism
596 in the Antigonish Highlands, Avalon terrane, Nova Scotia: tracking the evolution of the

597 mantle and crustal sources during the evolution of the Rheic Ocean. *Tectonophysics* 461,
598 181-201.

599

600 Murphy, J. B., Dostal, J., Gutierrez-Alonso, G., Keppie, J.D., 2011. Early Jurassic
601 magmatism on the northern margin of CAMP: derivation from a Proterozoic sub-
602 continental lithospheric mantle. *Lithos* 123, 158-164.

603

604 Murphy, J.B., Shellnutt, J.G., Collins, W.J., 2018. Late Neoproterozoic to Carboniferous
605 genesis of A-type magmas in Avalonia of northern Nova Scotia: repeated partial melting
606 of anhydrous lower crust in contrasting tectonic environments. *International Journal of*
607 *Earth Sciences* 107, 587-599.

608

609 Pilote, J.L., Barr, S.M., Wilson, R.A., McClenaghan, S., Kamo, S., McNicoll, V.J.,
610 Bevier, M.L., 2013. Precise age and petrology of Silurian-Devonian plutons in the
611 Benjamin River-Charlo area, northern New Brunswick. *Atlantic Geology* 48, 97-123.

612

613 Pollock, J.C., Hibbard, J.P., van Staal, C.R., 2012. A paleogeographical review of the
614 peri-Gondwanan realm of the Appalachian orogen. *Canadian Journal of Earth Sciences*
615 49, 259-288.

616

617 Pollock, J.C., Sylvester, P.J., Barr, S.M. 2015. Lu-Hf zircon and Sm-Nd whole-rock
618 isotope constraints on the extent of juvenile arc crust in the Avalonia: examples from

- 619 Newfoundland and Nova Scotia, Canada. *Canadian Journal of Earth Sciences* 52, 161-
620 181.
- 621
- 622 Riley, T.R., Lear, P.T., Pankhurst, R.J., Harris, C., 2001. Origins of large volume
623 rhyolitic volcanism in the Antarctic Peninsula and Patagonia by crustal melting. *Journal*
624 *of Petrology* 12, 1043-1065.
- 625
- 626 Rodgers, J., 1970. *The Tectonics of the Appalachians*. New York, John Wiley and Sons,
627 271 p.
- 628
- 629 Rudnick, R.L., Gao, S., 2003. Composition of the Continental Crust. *In*: Rudnick, R.L.
630 (Ed.) *The Crust. Treatise on Geochemistry*, 3, 1-64.
- 631
- 632 Schiano, P., Monzier, M., Eissen, J.P., Martin, H., Koga, K.T., 2010. Simple mixing as
633 the major control on the evolution of volcanic suites in the Ecuadorian Andes.
634 *Contributions to Mineralogy and Petrology* 160, 297-312.
- 635
- 636 Shellnutt, J.G., Jahn, B.M., Zhou, M.F., 2011. Crustal-derived granites in the Panzhihua
637 region, SW China: Implications for felsic magmatism in the Emeishan Large Igneous
638 province. *Lithos* 123, 145-157.
- 639
- 640 Sun, S.S., McDonough, W.F., 1989. Chemical and isotopic systematics of oceanic
641 basalts: implications for mantle composition and processes. *In*: Saunders, A.D., Norry,

- 642 M.J. (eds.) Magmatism in Ocean Basins. Geological Society London Special Publication
643 42, 313-345.
- 644
- 645 van Staal, C.R., de Roo, J.A. 1995. Mid-Paleozoic tectonic evolution of the Appalachian
646 Central Mobile Belt in northern New Brunswick, Canada: Collision, extensional collapse
647 and dextral transpression. *In*: Hibbard, J.P., van Staal, C.R., Cawood, P.A. (eds.). Current
648 Perspectives in the Appalachian-Caledonian Orogen. Geological Association of Canada,
649 Special Paper 41, 367-389.
- 650
- 651 van Staal, C.R., Hatcher, R.D., Jr., 2010. Global setting of Ordovician orogenesis. *In*:
652 Finney, S.C., Berry, W.B.N. (eds.) The Ordovician Earth System. Geological Society of
653 America, Special Paper 466, 1-11.
- 654
- 655 van Staal, C.R., Barr, S.M., 2012. Lithospheric architecture and tectonic evolution of the
656 Canadian Appalachians and associated Atlantic margin. Chapter 2. *In*: Percival, J.A.,
657 Cook, F.A., Clowes, R.M. (eds.). Tectonic Styles in Canada: the LITHOPROBE
658 Perspective. Geological Association of Canada, Special Paper 49, 41-95.
- 659
- 660 van Staal, C.R., Sullivan, R.W., Whalen, J.B., 1996. Provenance and tectonic history of
661 the Gander Zone in the Caledonian/Appalachian orogen: Implications for the origin and
662 assembly of Avalon. *In*: Nance, R.D., Thompson, M.D. (eds.) Avalonian and Related
663 Peri-Gondwanan Terranes of the Circum-North Atlantic: Geological Society of America
664 Special Papers 304, 347-367.

665

666 van Staal, C.R., Whalen, J.B., Valverde-Vaquero, P., Zagorevski, A., Rogers, N., 2009.

667 Pre Carboniferous, episodic accretion-related, orogenesis along the Laurentian margin of

668 the northern Appalachians. *In*: Murphy, J. B., Keppie, J.D., Hynes, A.J. (eds.) *Ancient*

669 *Orogens and Modern Analogues*. Geological Society of London Special Publication 327,

670 271-316.

671

672 van Staal, C.R., Barr, S.M., Murphy, J.B., 2012. Provenance and tectonic evolution of

673 Ganderia: Constraints on the evolution of the Iapetus and Rheic Oceans. *Geology* 40,

674 987–990.

675

676 Waight, T.E., Wiebe, R.A., Krogstad, E.J., 2007. Isotopic evidence for multiple

677 contributions to felsic magma chambers: Gouldsboro, Coastal Maine. *Lithos* 93, 234-247

678

679 Waldron, J.W.F., Schofield, D.I., Murphy, J.B., Thomas, C.W., 2014. How was the

680 Iapetus Ocean infected with subduction? *Geology* 42, 1095-1098, doi:10.1130/G36194.1

681

682 Walker, J.A., McCutcheon, S.R., 1995. Siluro-Devonian stratigraphy of the Chaleur Bay

683 Synclinorium, northern New Brunswick. *In*: *Current Research 1994*. New Brunswick

684 Department of Natural Resources and Energy, Minerals and Energy Division,

685 Miscellaneous Report 18, 225-244.

686

687 Wang, F., Li, Q., Liu, Y., Jiang, S., Chen, C., 2019. Geochronology of magmatism and
688 mineralization in the Dongbulage Mo-polymetallic deposit, Northwest China:
689 Implications for the timing of mineralization and ore genesis. *Minerals* 9, 255.
690 Doi:10.3390/min9050255.

691

692 Watson, E.B., Harrison, T.M., 1983. Zircon saturation revisited: temperature and
693 composition effects in a variety of crustal magma types. *Earth Planetary Science Letters*
694 64, 295-304.

695

696 Whalen, J. B., Jenner, G.A., Hegner, E., Garipey, C., Longstaffe, F.J., 1994. Geochemical
697 and isotopic (Nd, O and Pb) constraints on granite sources in the Humber and Dunnage
698 zone, Gaspesie, Quebec, and New Brunswick: implications for tectonics and crustal
699 structure. *Canadian Journal of Earth Sciences* 31, 323-340.

700

701 Whalen, J.B., Jenner, G.A., Longstaffe, F.J., Hegner, E., 1996. Nature and evolution of
702 the eastern margin of Iapetus: geochemical and isotopic constraints from Siluro-Devonian
703 granitoid plutons in the New Brunswick Appalachians. *Canadian Journal of Earth*
704 *Sciences* 33, 140-155.

705

706 Whalen, J.B., Hildebrand, R.S., 2019. Trace element discrimination of arc, slab failure,
707 and A-type granitic rocks. *Lithos*, 348-349.

708

- 709 Whalen, J.B., Currie, K.L., Chappell, B.W., 1987. A-type granites; geochemical
710 characteristics, discrimination and petrogenesis. *Contributions to Mineralogy and*
711 *Petrology*, 95, 407-419.
- 712
- 713 Wilson, R.A., 2017. The Middle Paleozoic rocks of northern and western New
714 Brunswick, Canada. New Brunswick Department of Energy and Resource Development,
715 Geological Surveys Branch, Memoir 4, 319 p.
- 716
- 717 Wilson, R.A., Kamo, S., 2008. New U-Pb ages from the Chaleurs and Dalhousie groups:
718 Implications for regional correlations and tectonic evolution of northern New Brunswick.
719 *In: Martin, G.L. (ed.). Geological Investigations in New Brunswick for 2007. New*
720 *Brunswick Department of Natural Resources; Minerals, Policy and Planning Division,*
721 *Mineral Resource Report 2008-1, 55-77.*
- 722
- 723 Wilson, R.A., Kamo, S.L., 2012. The Salinic Orogeny in northern New Brunswick:
724 Geochronological constraints and implications for Silurian stratigraphic nomenclature.
725 *Canadian Journal of Earth Sciences* 49, 222-238.
- 726
- 727 Wilson, R.A., Kamo, S.L. 2016. Geochronology and lithochemistry of granitoid rocks
728 from the central part of the Central plutonic belt, New Brunswick, Canada: implications
729 for Sn-W-Mo exploration. *Atlantic Geology* 52, 125-167.
- 730

- 731 Wilson, R.A., van Staal, C.R., Kamo, S. L., 2017. Rapid transition from the Salinic to
732 Acadian orogenic cycles in the Northern Appalachian orogen: evidence from Northern
733 New Brunswick, Canada. *American Journal of Science* 317, 448-481.
734
- 735 Wilson, R.A., Burden, E.T., Bertrand, R., Asselin, E., McCracken, A.D., 2004.
736 Stratigraphy and tectono-sedimentary evolution of the Late Ordovician to Middle
737 Devonian Gaspé Belt in northern New Brunswick: Evidence from the Restigouche area.
738 *Canadian Journal of Earth Sciences* 41, 527-551.
739
- 740 Wilson, R.A., Kamo, S., Burden, E.T., 2005. Geology of the Val d'Amour Formation:
741 Revisiting the type area of the Dalhousie Group, northern New Brunswick. *In:* Martin,
742 G.L. (ed.) *Geological Investigations in New Brunswick for 2004*. New Brunswick
743 Department of Natural Resources; Minerals, Policy and Planning Division, Mineral
744 Resource Report 2005-1, 167-212.
745
- 746 Winchester, J.A. and Floyd. P.A. 1977. Geochemical discrimination of different magma
747 series and their differentiation products using immobile elements. *Chemical Geology*, 20,
748 325-343.
749
- 750 Wu, F.Y., Jahn, B.M., Wilde, S.A., Lo, C.H., Yui, T.F., Lin, Q., Sun, D.Y., 2003. Highly
751 fractionated I-type granites in NE China (I): geochronology and petrogenesis. *Lithos* 66,
752 241-273.
753

754 Xia, Y., Xu, X., Liu, L., 2016. Transition from adakitic to bimodal magmatism induced
755 by the paleo-Pacific plate subduction and slab rollback beneath SE China: evidence from
756 petrogenesis and tectonic setting of the dike swarms. *Lithos* 244, 182-204.

757

758 Zagorevski, A., van Staal, C.R., Rogers, N., McNicoll, V., Dunning, G.R., Pollock, J.C.,
759 2010. Middle Cambrian to Ordovician arc-backarc development on the leading edge of
760 Ganderia, Newfoundland Appalachians. *In*: Tollo, R.P. (ed.) *From Rodinia to Pangea:*
761 *The lithotectonic record of the Appalachian region.* Geological Society of America
762 *Memoir* 206, 367-396.

763

764

765 **Table captions**

766

767 Table 1. Nd isotopic composition of volcanic rocks of the Dickie Cove Group.

768

769 Table 2 Zircon and monazite saturation thermometry estimates of rhyolitic rocks of
770 Dickie Cove Group.

771

772

773 **Figure captions**

774

775 Figure 1. Major lithotectonic domains of the northern Appalachians (modified after van
776 Staal and Barr, 2012 and Dostal et al., 2016). NB: New Brunswick.

777

778 Figure 2. (A) Simplified geology of the Chaleur Bay Synclinorium and adjacent inliers in
779 New Brunswick (modified from Wilson et al., 2017). U-Pb zircon dates from Silurian to
780 Lower Devonian felsic volcanic rocks of the Tobique and Dickie Cove groups are
781 indicated, as well as from the Silurian Landry Brook [LB] pluton and Silurian-Lower
782 Devonian Dickie Brook [DB] pluton, both of which intrude the Dickie Cove Group. Data
783 from (1) Wilson and Kamo (2008), (2) Wilson and Kamo (2012), (3) Pilote et al. (2013),
784 and (4) Wilson et al. (2017). (B) Areal extent of the Chaleur and Tobique zones, which
785 are respectively to the north and south of the Rocky Brook - Millstream Fault. (C)
786 Stratigraphic columns showing the age of Silurian to Lower Devonian volcanic rocks of
787 the Dickie Cove, Tobique and Dalhousie groups in the Chaleur Zone and in the northern
788 part of the Tobique Zone.

789

790 Figure 3. Zr/TiO₂ versus Nb/Y classification diagram for the DCG bimodal suite
791 (modified from Winchester and Floyd, 1977). Fields: TA - Trachyandesite; Alk-Bas -
792 Alkali basalt.

793

794 Figure 4. Fe* [(FeO*/(FeO*+MgO))] versus SiO₂ (wt.%) for the DCG rhyolitic rocks
795 showing the separation of ferroan and magnesian rocks (after Frost et al. 2001).

796

797 Figure 5. (A) 10,000xGa/Al versus Zr (ppm) diagram (after Whalen et al., 1987) for the
798 DCG rhyolitic rocks classifying them as A-type rocks. Fields: I&S field is for I- and S-
799 type granites while the A field is for the A-type granites. (B) Y+Nb (ppm) versus La/Yb

800 discrimination diagram of Whalen and Hildebrand (2019) showing the A-type
801 characteristics of the DCG felsic volcanic rocks.

802

803 Figure 6. Chondrite-normalized rare-earth element diagrams for the DCG rocks (A)
804 rhyolitic rocks; (B) basaltic rocks (after Dostal et al., 2016). Normalizing values are after
805 Sun and McDonough (1989).

806

807 Figure 7. Primitive-mantle normalized incompatible element abundances for the DCG
808 rocks: (A) rhyolitic rocks, (B) basaltic rocks (after Dostal et al., 2016). Elements are
809 arranged in the order of decreasing incompatibility from left to right. Normalizing values
810 are after Sun and McDonough (1989).

811

812 Figure 8. TiO_2 (wt.%) versus FeO^*/MgO diagram for the DCG rocks. Vectors depict
813 tholeiitic and calc-alkali fractionation trends (after Miyashiro, 1974). FeO^* - total Fe as
814 FeO .

815

816 Figure 9. Y-Nb-Ce diagram for the DCG rhyolitic rocks discriminating between A1 and
817 A2-types of anorogenic granites (Eby, 1992). A1-type anorogenic granites related to ocean
818 island-type sources; A2-type anorogenic granites derived from continental crust sources.

819

820 Figure 10. (A) Chondrite-normalized La/Yb ratio versus La (ppm) diagram for the DCG
821 felsic rocks. Fractionation vectors for accessory minerals are after Wu et al. (2003).

822 Mineral vectors are based on fractionation of monazite (Mon), allanite (Allan), apatite

823 (Ap), titanite (Tit) and zircon (Zr). (B) Variations of Th/Nb versus Zr (ppm) in the DCG
824 rhyolitic rocks showing the vectors for increasing fractional crystallization (FC),
825 combined assimilation-fractional crystallization (AFC) and source heterogeneity
826 (modified after El-Bialy and Hassen, 2012).

827

828 Figure 11. (A) Variations of Ba (ppm) versus Eu/Eu* in the DCG rhyolitic rocks. Eu
829 anomalies are calculated as (Eu/Eu*) where Eu denotes the chondrite-normalized value
830 and Eu* represents the Eu value expected for a smooth chondrite-normalized REE
831 pattern. (B). Variations of Ba/Zr versus Ba (ppm) in the DCG rhyolitic rocks showing
832 the vectors for fractional crystallization and partial melting (after Schiano et al. 2010 and
833 Wang et al. 2019).

834

835 Figure 12. $\epsilon_{Nd}(t)$ versus time plot comparing Sm-Nd isotopic data of the DCG and TG
836 rhyolitic rocks with basaltic rocks of Avalonia (Keppie et al., 1997; Murphy et al., 2011)
837 and Ganderia (Dostal et al., 2016, 2020) of Nova Scotia and New Brunswick. Shaded
838 area (envelope) is the Avalonian basement and SCLM (after Keppie et al., 2012; Murphy
839 et al., 2011, 2018). The field for Mesoproterozoic rocks is from Murphy et al. (2008).
840 CHUR- chondritic uniform reservoir.

841

842 Figure 13. Tectonic model for Silurian volcanism in the northern Appalachians. (A)
843 Closure of the Tetagouche-Exploits back-arc basin and deposition of forearc rocks of the
844 Matapedia cover sequence (MCS) following the Upper Ordovician accretion of
845 Ganderia's leading edge (the Popelogan arc) to Laurentia. (B) Closure of the back-arc

846 basin culminating with the Wenlock-Ludlow Salinic Orogeny and initial deposition of the
847 syn-orogenic Petit Rocher Group in northern New Brunswick. (C) Pridolian mafic
848 magmatism triggered by detachment of the Tetagouche-Exploits slab (TES), post-
849 orogenic root relaxation, and partial melting of the sub-continental lithospheric mantle
850 (SCLM). Felsic melts were in turn produced at the base of the crust by heat derived from
851 mafic underplating. The Dickie Cove Group (DCG) rhyolites of the Chaleur Zone were
852 ultimately sourced from felsic diapirs issued from the base of the crust. (D) Extensional
853 collapse of the Salinic root later in the Pridolian, and expansion of the volcanic belt to
854 form a distinct volcanic suite in the Tobique Zone.

Figure 1

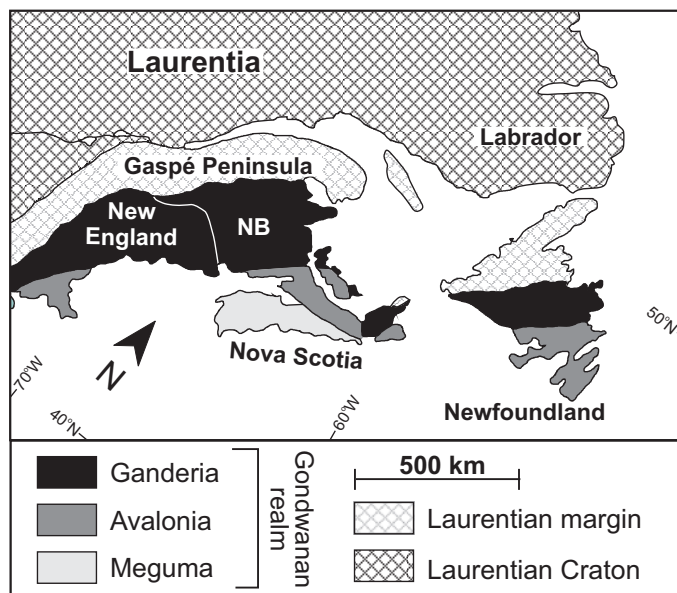


Fig. 1

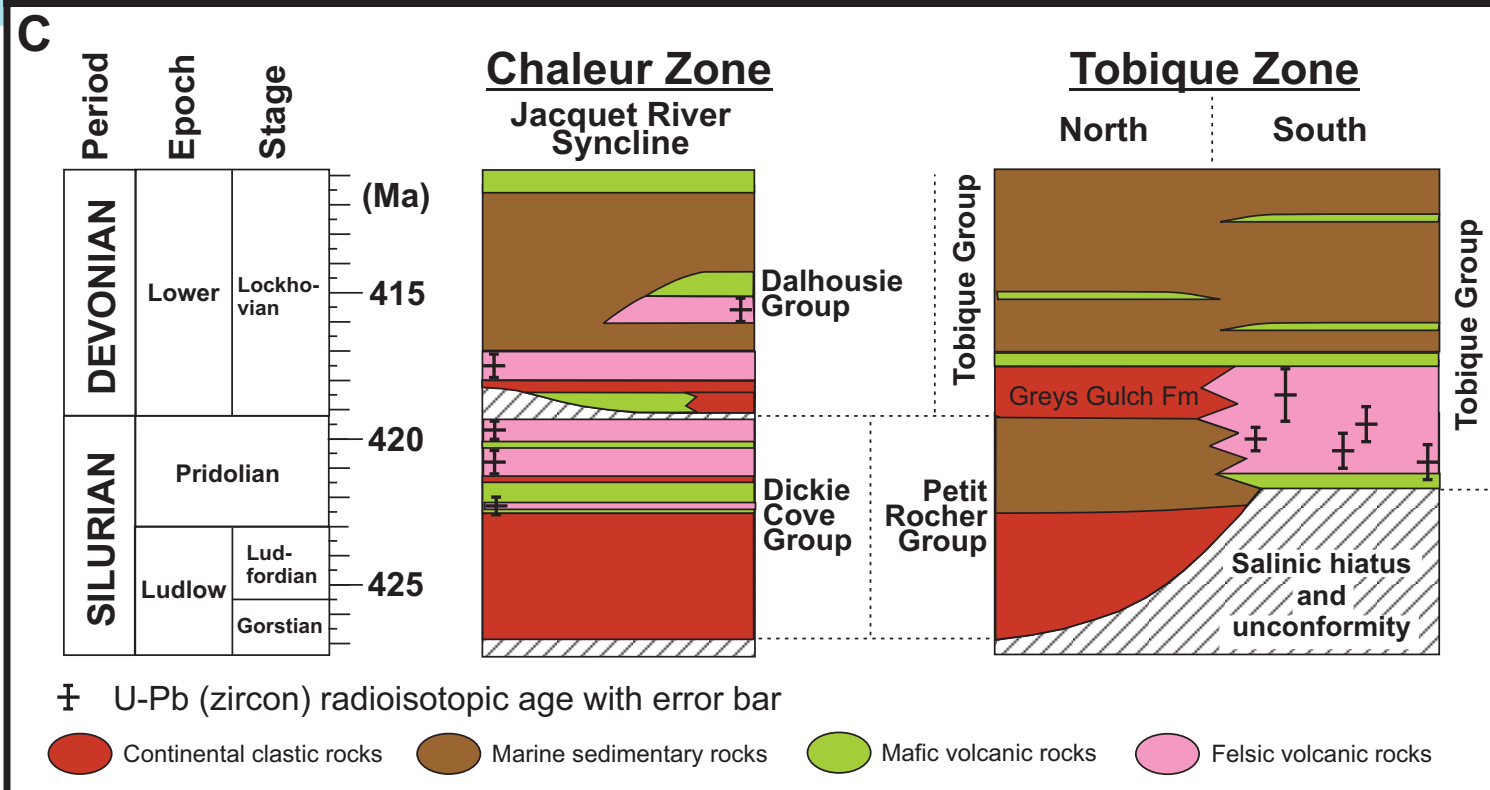
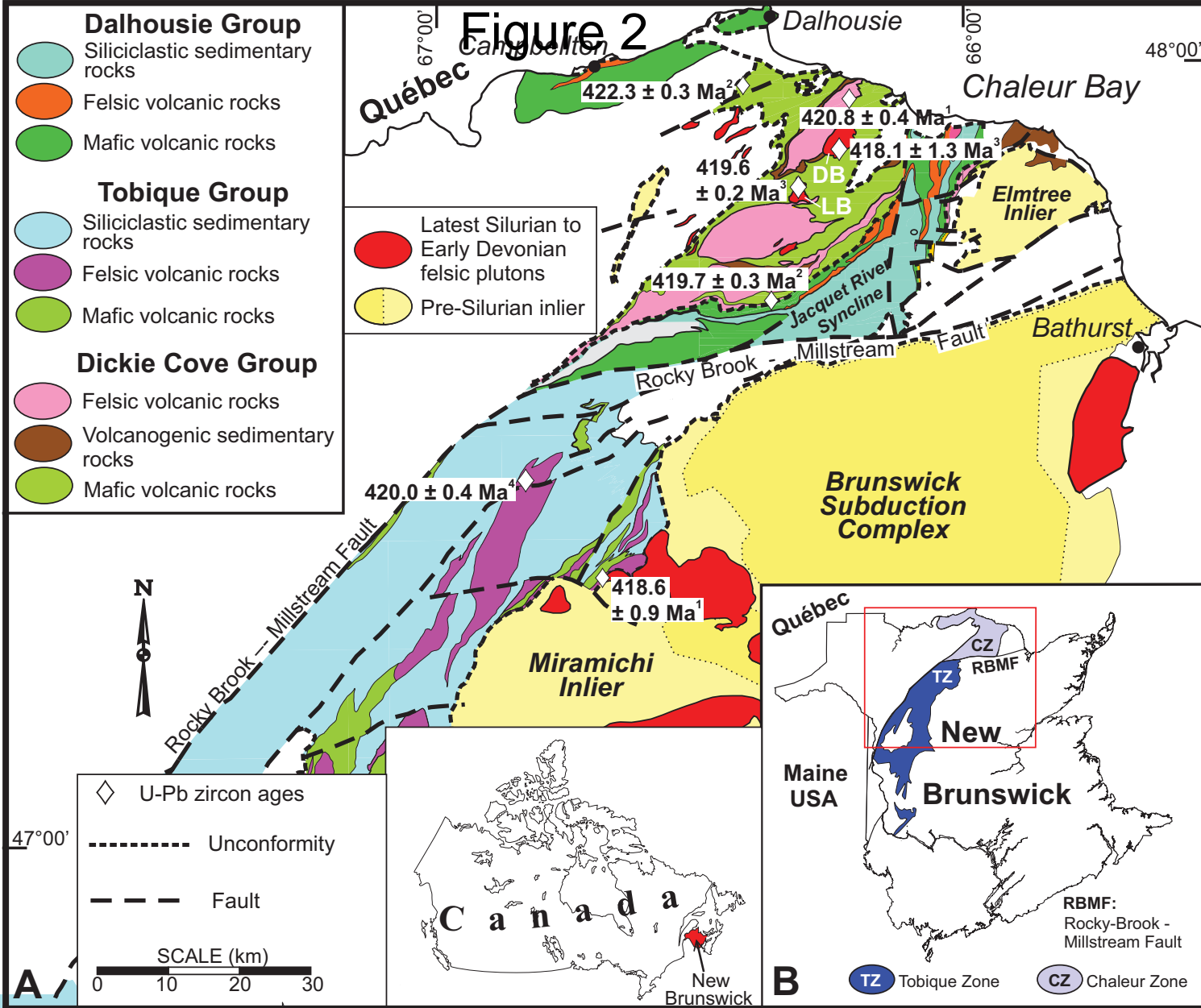


Fig. 2

Figure 3

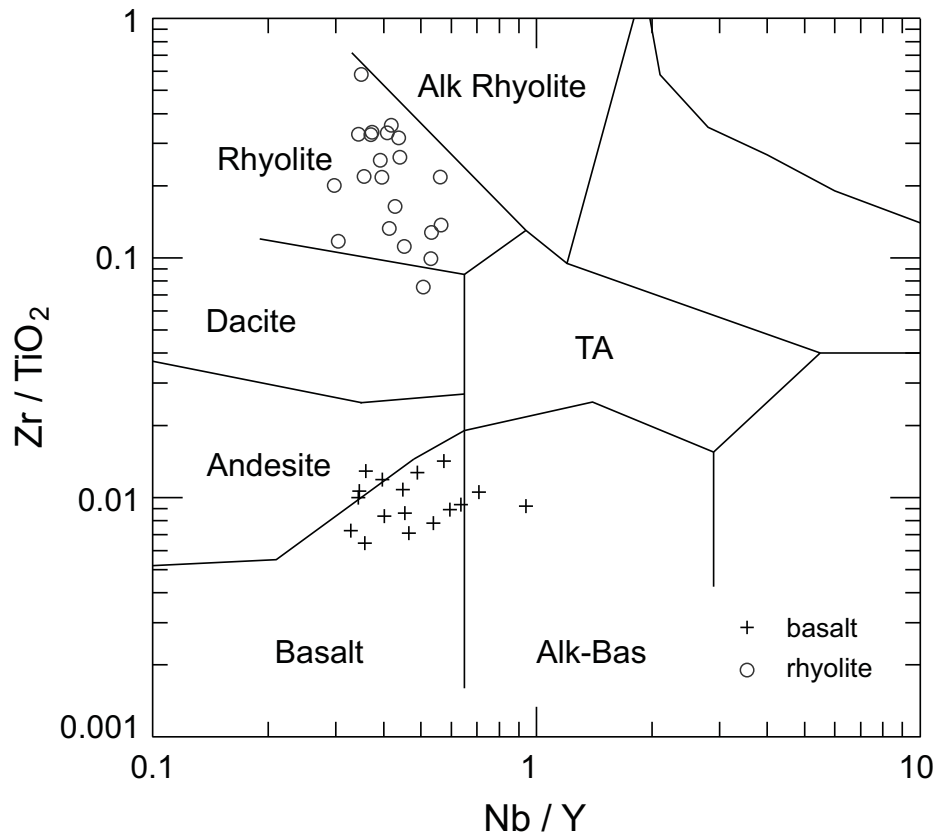


Figure 4

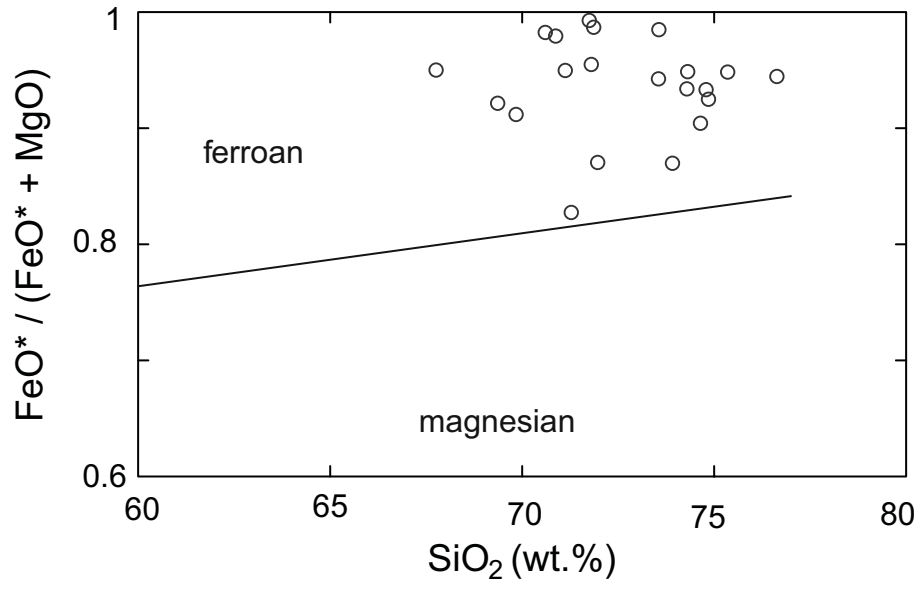


Figure 5A

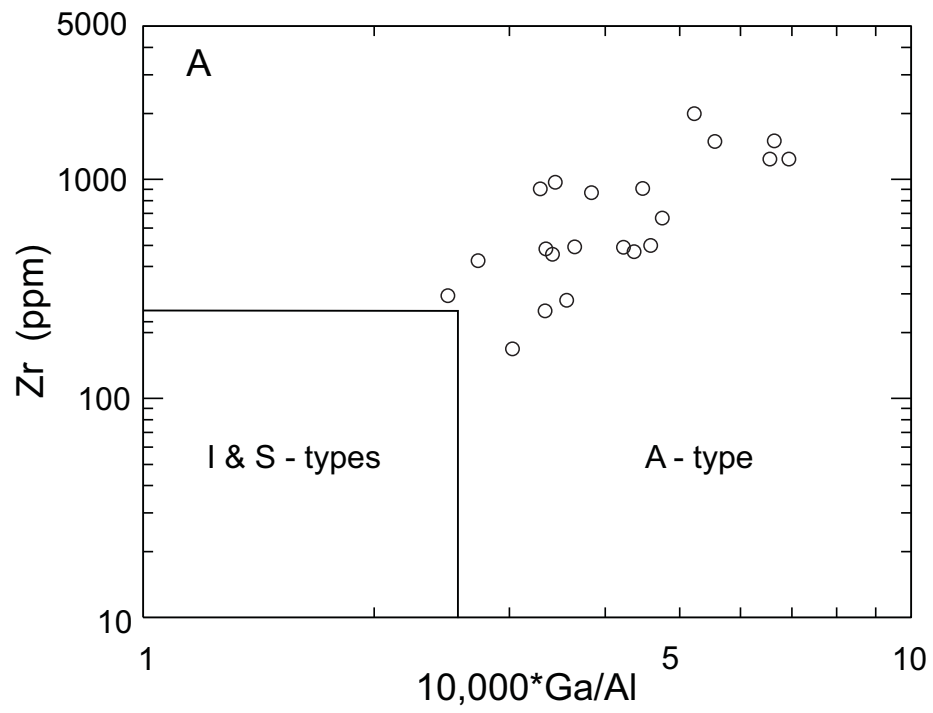


Figure 5B

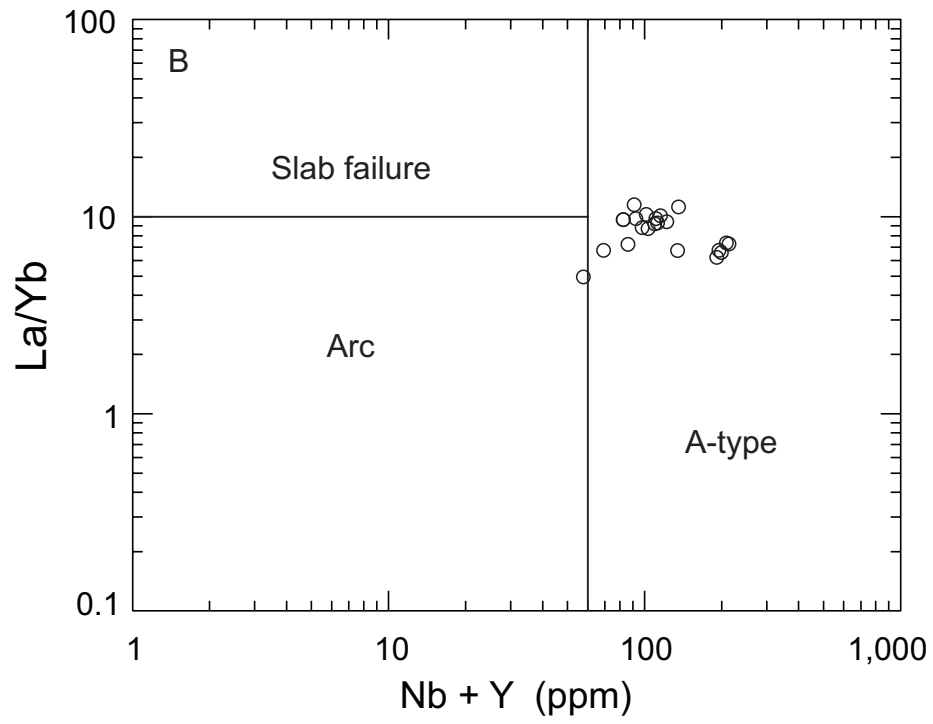


Figure 6A

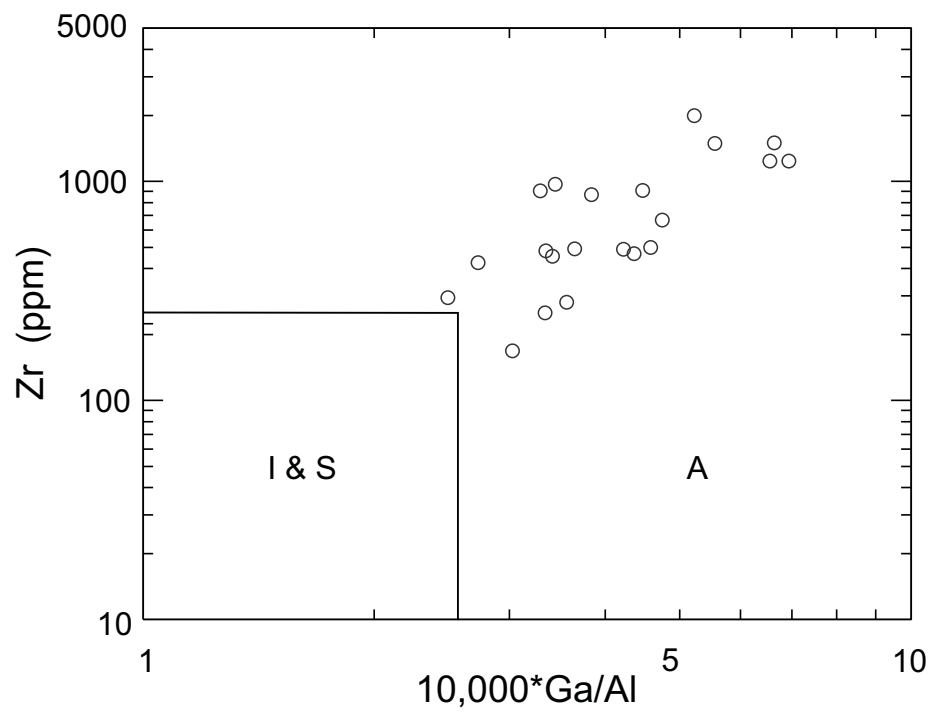


Figure 6B

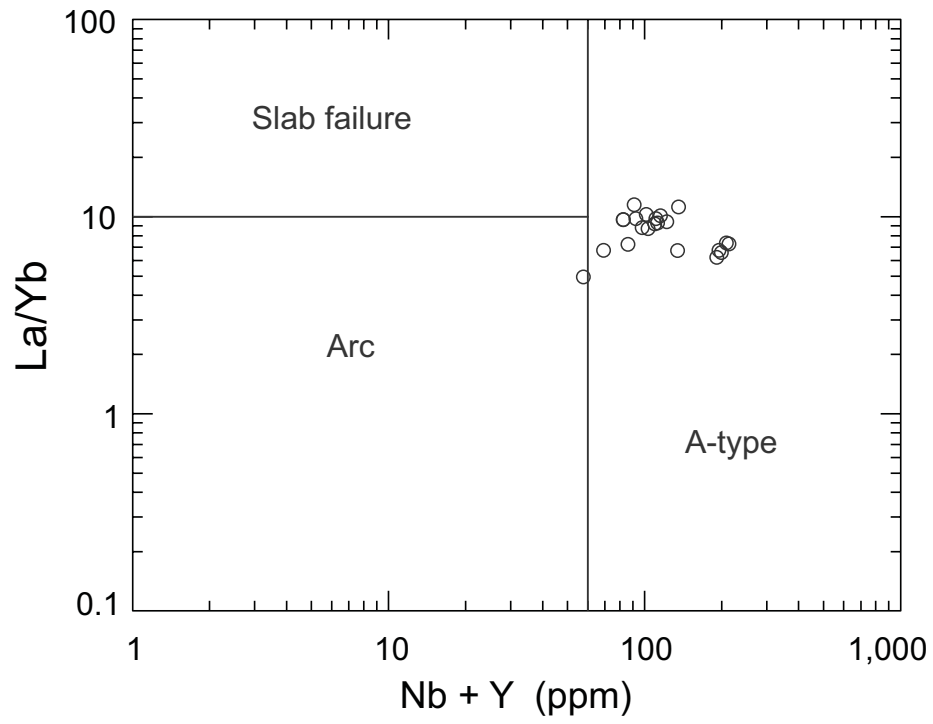


Figure 7

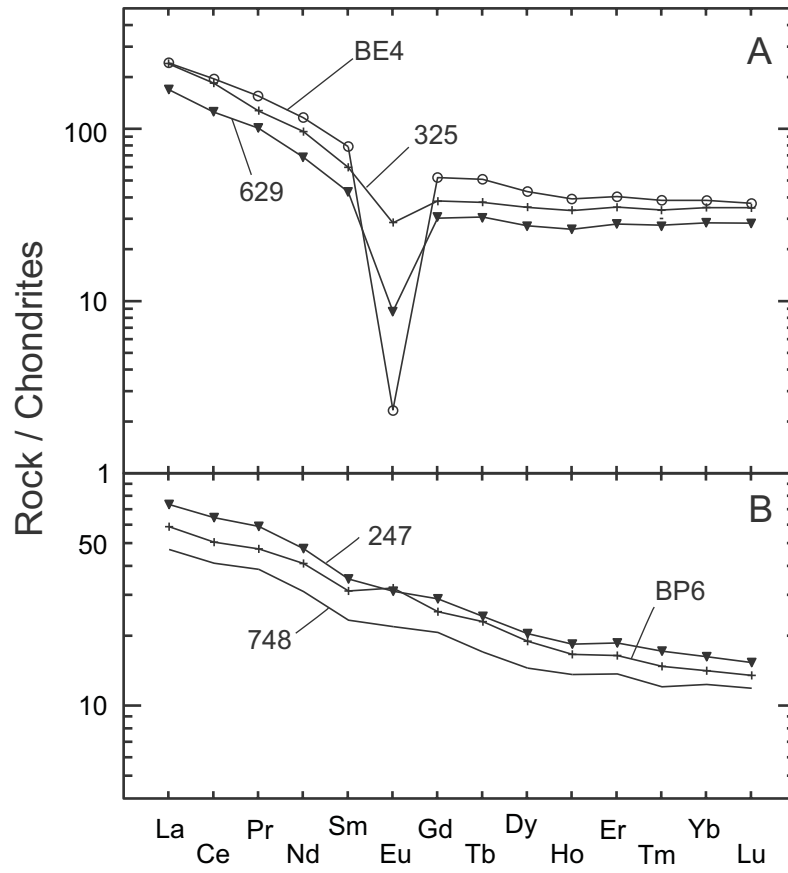


Figure 8

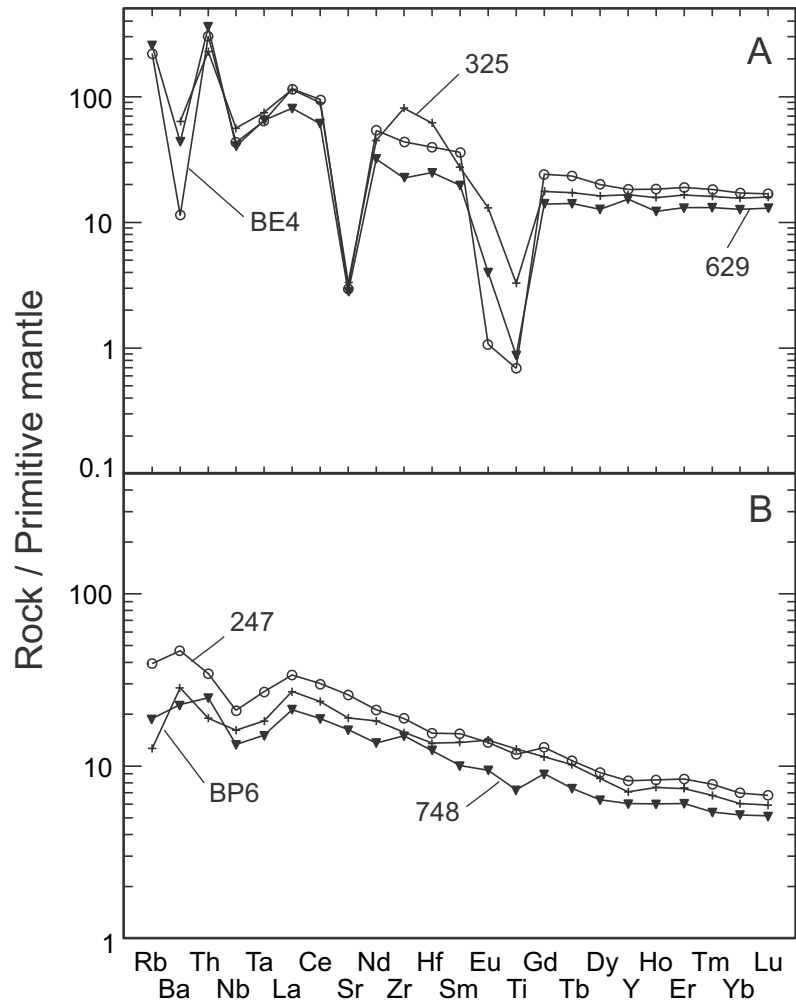


Figure 9

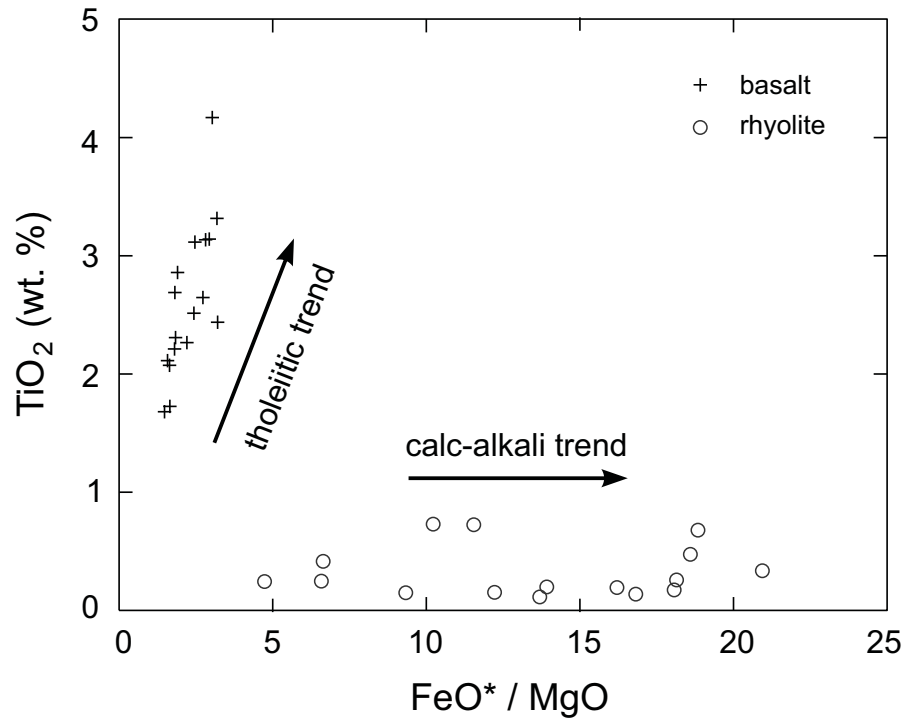


Figure 10A

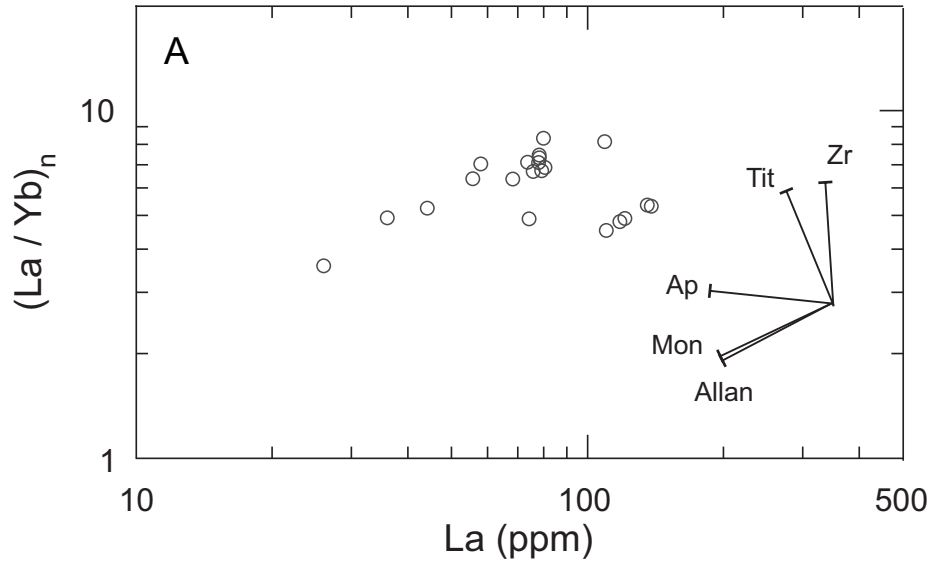


Figure 10B

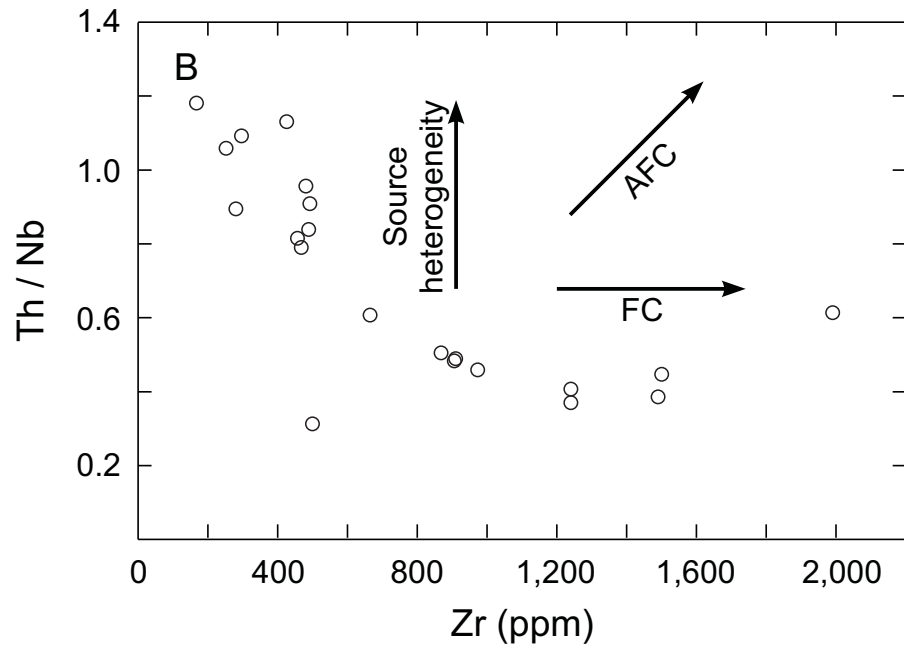


Figure 11A

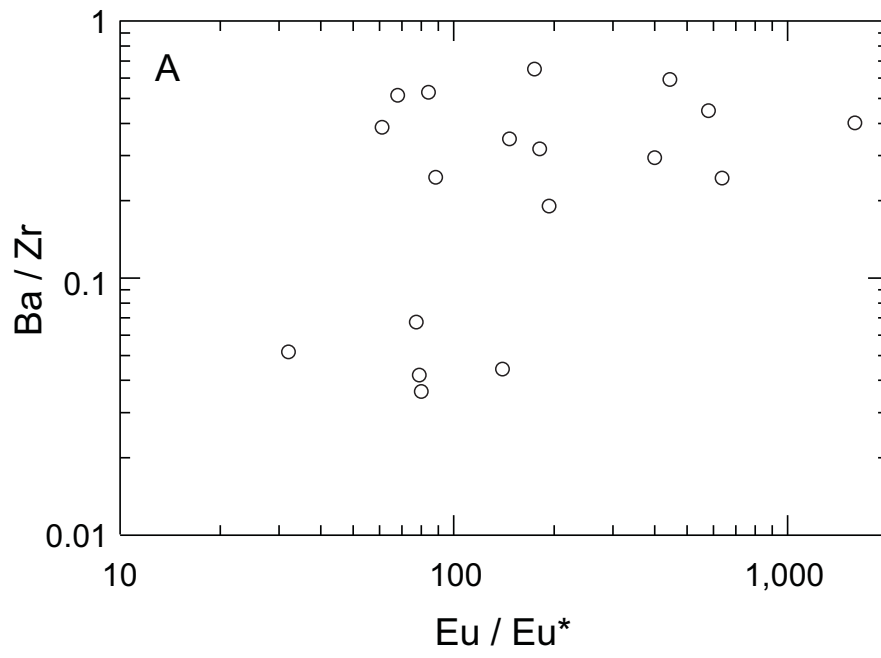


Figure 11B

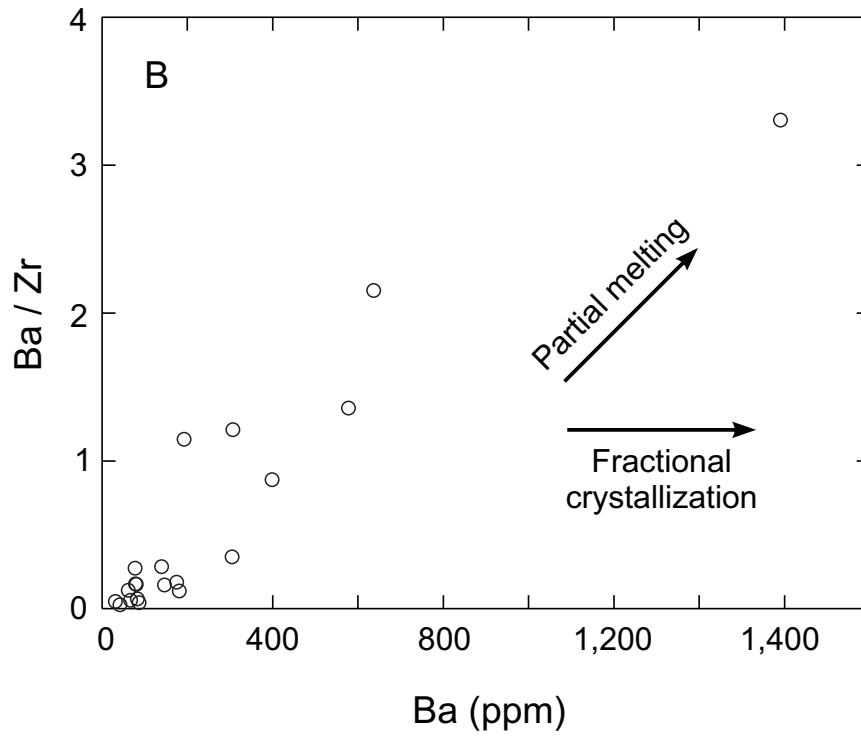
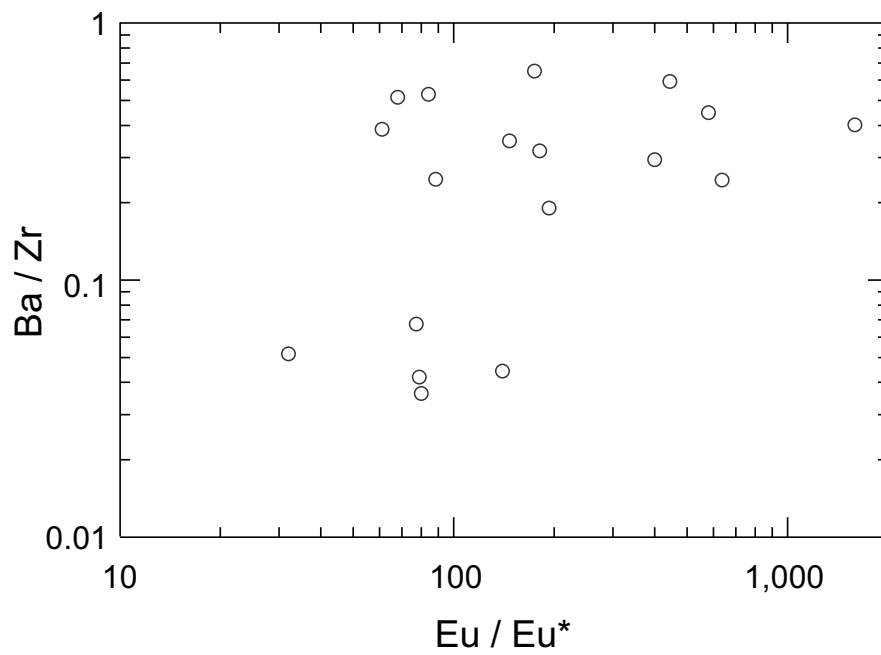


Figure 12



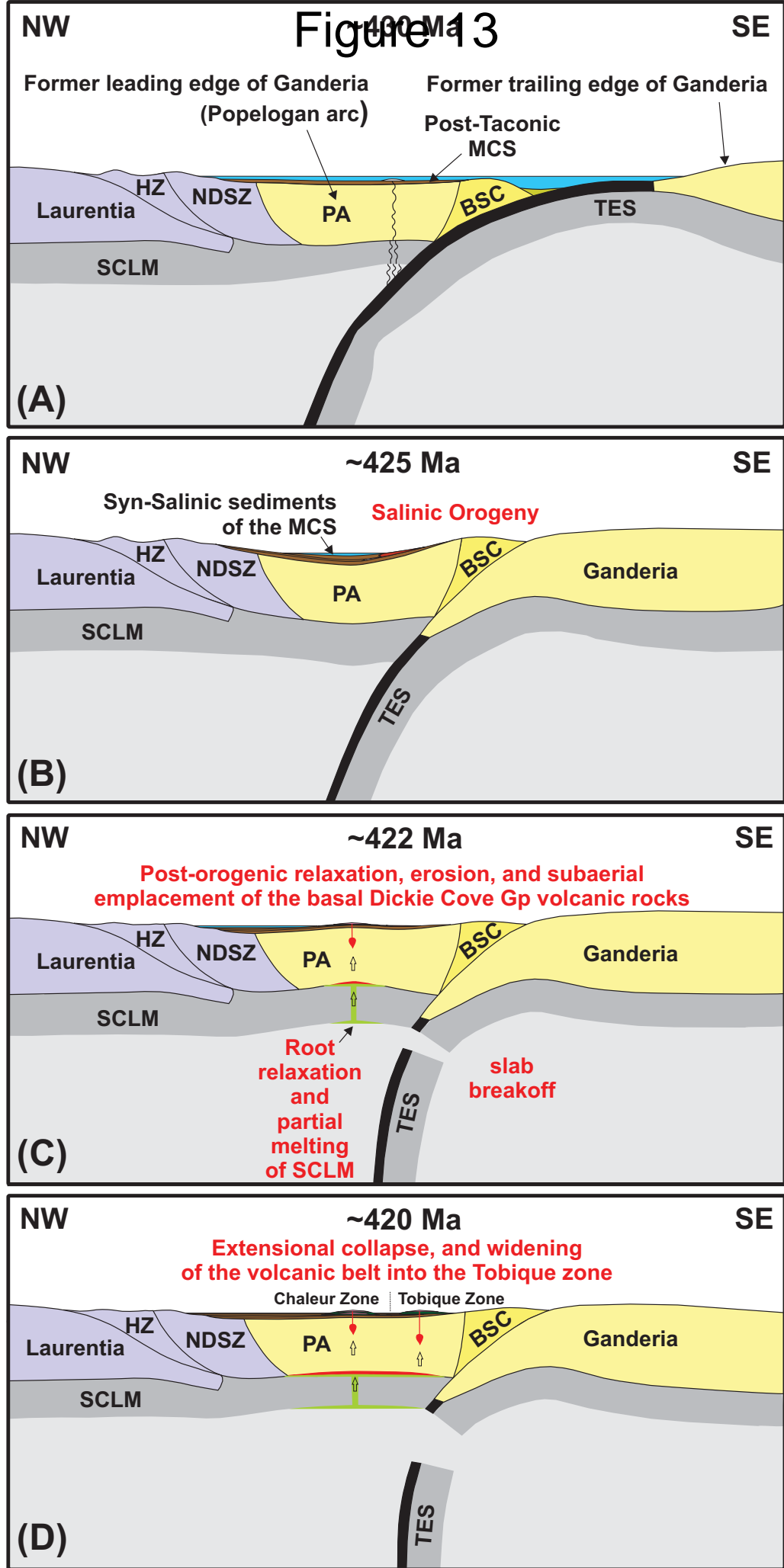


Fig. 13

Table 1. Nd isotopic composition of volcanic rocks of the Dickie Cove Group

Sample	Age (Ma)	Nd(ppm)	Sm(ppm)	$^{147}\text{Sm}/^{144}\text{Nd}$	$^{143}\text{Nd}/^{144}\text{Nd}_{(m)}$	2σ	$^{143}\text{Nd}/^{144}\text{Nd}_{(i)}$	$\epsilon_{\text{Nd}(t)}$	T_{DM} (Ma)
207	421	81.49	16.44	0.1219	0.512469	7	0.512133	0.73	958
402	421	36.57	8.09	0.1337	0.512556	7	0.512187	1.79	934
285	421	65.13	12.88	0.1196	0.512598	7	0.512268	3.37	733
629	421	45.21	9.36	0.1253	0.512524	6	0.512179	1.62	901
PB6*	421	23.87	5.82	0.1475	0.512769	6	0.512362	5.21	652
247*	421	28.01	6.48	0.1400	0.512653	7	0.512267	3.35	818
748*	421	18.35	4.25	0.1402	0.512694	6	0.512307	4.14	738

T_{DM} -depleted mantle model age calculated using the model of DePaolo (1988). $\epsilon_{\text{Nd}(t)}$ - age-corrected values for the 421 Ma);

crystallization age ($t = 143\text{Nd}/144\text{Nd}_{(m)}$)- measured value; $^{143}\text{Nd}/^{144}\text{Nd}_{(i)}$ - initial, calculated value;

*-after Dostal et al. (2016)

Table 2 Zircon and monazite saturation thermometry estimates of rhyolitic rocks of Dickie Cove Group

	177	629	BE3	BE4	BR5	207	266	285	325	402
M	1.28	1.28	1.32	1.4	1.36	1.26	1.59	1.25	0.06	1.33
T _{Zr} ^{°C}			873	867	874		1006			869
T _{Mz} ^{°C}	869	841	866	859	861	904	913	872	926	822
	482	204	278	C-1	C-3	C-6	C-7	19	23	17
M	1.28	1.17	1.39	1.87	1.86	1.74	1.57	1.27	1.54	1.57
T _{Zr} ^{°C}			954	945	919	968	1047		975	845
T _{Mz} ^{°C}	808	897	863	807	799	834	867	778	866	817

M = [Na+K+2Ca] / [Al*Si]; T_{Zr}^{°C} = zircon saturation temperature calculated according to

Boehnke et al. (2013);

TMzoC = monazite saturation temperature calculated according to Montel (1993).